Journal of Luminescence 170 (2016) 841–854

Contents lists available at ScienceDirect

Journal of Luminescence

journal homepage: www.elsevier.com/locate/jlumin

Efficient luminescence extraction strategies and anti-reflective coatings to enhance optical refrigeration of semiconductors

I. Hassani Nia, M. Rezaei, R. Brown, S.J. Jang, A. Turay, V. Fathipour, H. Mohseni *

Bio-inspired Sensors and Optoelectronics Laboratory (BISOL), Department of Electrical Engineering and Computer Science, Northwestern University, Evanston, IL 60208, USA

ARTICLE INFO

Article history:
Received 3 May 2015
Received in revised form
22 August 2015
Accepted 26 August 2015
Available online 3 September 2015

Keywords:
Anti-Stokes laser cooling
Extraction efficiency
External quantum efficiency

ABSTRACT

Laser refrigeration of solids has emerged as a viable solution for vibration-free and compact cooling that does not require any moving parts or cryogenic liquid. So far, rare-earth doped glasses are the only bulk materials that have provided efficient laser cooling based on the anti-Stokes process. These materials have low indices of refraction and are suitable for efficient luminescence extraction. However, up until this date, laser cooling of bulk semiconductors has not been achieved. One major challenge that needs to be addressed is the photoluminescence trapping and the consequent photon recycling. In this paper, we explain various methods to enhance light extraction for the purpose of laser cooling. We specifically provide guidelines for design and fabrication of graded index and subwavelength structures to maximize the extraction efficiency. Furthermore we present novel techniques for increasing the external quantum efficiency and enhancing the overall laser cooling efficiency.

© 2015 Elsevier B.V. All rights reserved.

1. Introduction

Luminescence extraction from materials has been one of the most important issues in optics over the past decades. In many fields of research such as biology, energy-saving solid-state devices (such as light emitting diodes and solar cells) and photonic devices, efficient coupling of light across different media is required to achieve sufficiently sensitive, accurate, and fast optical functionalities and to increase the efficiency of energy conversion. Light emission and absorption are dependent on the internal chemical and physical characteristics of the material as well as its structural characteristics that determine the coupling of the light from the active medium to the outside world [1–5]. In this regard, various techniques have been attempted to increase light coupling. These methods rely on surface modifications, deposition of anti-reflective (AR) coatings, or changes of the size and shape of the material in order to enhance the light coupling. Here, we review the main strategies for increasing light extraction and outline their advantages and drawbacks in the context of optical refrigeration of semiconductors. However, many of the strategies detailed here could be directly used in the aforementioned fields.

Laser cooling has emerged as a vibration free, robust and compact technique of cooling that can achieve temperatures below 100 K [6], clearly surpassing its technological counterpart, the thermoelectric cooler, which at best reaches ~170 K [7]. Various techniques to refrigerate solids with lasers have been proposed. These include Coulomb assisted laser cooling in piezoelectric materials [8], luminescence-up conversion (known as anti-Stokes optical refrigeration [9]), frequency down-conversion [10] and super-radiance [11] to name a few. However, anti-Stokes has been the dominant mechanism used for laser cooling of condensed matter [9,12–18]. Although anti-Stokes optical refrigeration is the subject of this study, efficient luminescence extraction is required to increase the cooling efficiency of all of the aforementioned laser cooling methods. The anti-Stokes mechanism is schematically shown in Fig. 1. The laser source, which is tuned slightly below the bandgap, produces electrons at the bottom of conduction band and holes at the top of the valence band. These carriers interact with the phonons and scatter to the empty energy states. After reaching equilibrium, i.e. once they thermalize with the phonons, the average electron energy increases by kT where k is the Boltzmann constant and T is the temperature. Therefore, at equilibrium the average energy of the emitted photons by radiative recombination is higher than the absorbed laser photons. In this process, if all of the photogenerated carriers undergo radiative recombination and all the luminescence energy transfers out of the material, there will always be a net energy extraction (i.e. net cooling). The energy extraction results in the temperature drop and continues up to a point where kT becomes so small that laser cooling power gets balanced by the heating produced due to parasitic absorption of the laser. The first observation of such a phenomenon was not realized experimentally until 1995, in

* Corresponding author. Tel.: +1 847 491 7108.
E-mail address: hmohseni@ece.northwestern.edu (H. Mohseni).

http://dx.doi.org/10.1016/j.jlumin.2015.08.051
0022-2313/© 2015 Elsevier B.V. All rights reserved.

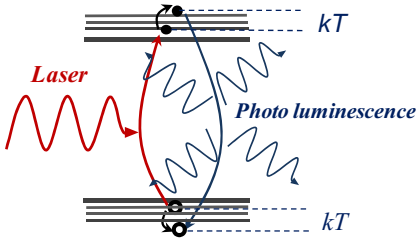

Fig. 1. Illustration of anti-Stokes laser cooling. The energy diagram that illustrates the basic idea of anti-Stokes laser cooling.

trivalent ytterbium ion doped heavy-metal-fluoride glass [19]. In rare earth ions, the electronic 4f levels are shielded from the surrounding by the filled 5s and 5p shells, leading to suppression of multi-phonon relaxation [20] and a high radiative recombination rate favorable for optical refrigeration. In addition, the refractive index of the host material is close to the refractive index of air providing a good extraction efficiency. It should be noted that in practice, there are non-radiative pathways that the carriers can undergo and produce heat. For semiconductors, there are two main mechanisms for non-radiative recombination: Shockley–Reed–Hall (SRH) and Auger recombination [21]. SRH recombination occurs due to interaction of the carriers with crystal non-idealities such as impurities, defects, and surface states. SRH recombination can be suppressed by enhancing the quality of the crystalline structure and by passivation of the surface. Auger recombination is a three-carrier coulomb scattering process that becomes significant at high carrier densities while the SRH mechanisms become predominant at low carrier densities. Therefore, the laser intensity and the carrier density should be kept at an optimum level to suppress both Auger and SRH recombination mechanisms [21]. To have a better understanding, we recall that the external quantum efficiency is defined as [22]

$$\eta_{ex} = \frac{\eta_e B n^2}{An + \eta_e B n^2 + Cn^3} \tag{1}$$

in which B is the binomial radiative coefficient, n is the carrier density, A and C are SRH and Auger recombination coefficients respectively. η_e is the extraction efficiency, which is equal to the fraction of the optical power extracted from the material to the total generated optical power inside the material. Cooling efficiency can be subsequently calculated as [22]

$$\eta_c = \eta_{abs}\eta_{ex}\frac{E_f}{E_i} - 1 \tag{2}$$

where E_i is the energy of the pump laser photons and E_f is the average energy of the emitted photons. η_{abs} is the absorption efficiency and is equal to [23]

$$\eta_{abs} = \frac{\alpha}{\alpha + \alpha_b} \tag{3}$$

where α is the aborption coefficent of the pump photons in the active region and α_b is the absorption of the pump photons in the rest of the material and is called background absorption. Eqs. (1) and (2) imply that in order to maximize the cooling efficiency the extraction efficiency should be maximized. This is due to the fact that if the photons get reabsorbed, then a portion of the resulting electrons and holes go through non-radiative recombination mechanism. As a result, heat is produced and significant reduction of the net extracted energy and cooling efficiency follows.

Photons can get trapped inside a material due to the total internal reflection and Fresnel reflection. However the optical energy cannot be stored in the material forever. Even in the case of perfect flat edges the angle of rays is not going to be conserved and the rays diverge due to diffraction and finally the energy is extracted out. Moreover because of the presence of an absorbing medium inside the structure, a portion of the energy is reabsorbed since the emission is associated with absorption [24]. These mechanisms result in the reduction of the output photon flux and the net extracted power. Therefore, effective strategies to reduce photon trapping are needed to assist laser cooling. We note that when the size of the structure becomes comparable to wavelength, then the above simple picture for bulk materials is not valid and a full solution of the electromagnetic wave equations is required. But even in that case the index and the size of the structure determines the amount of the power radiated out of the material in a similar fashion. For instance the higher the index and size of the material the higher the localization of the optical mode inside the material. Along the same lines, it has been shown that both the thickness and refractive index are critical for laser cooling of subwavelength cadmium sulfide nanobelts [25]. The escape cone for a bulk material with index n and air is equal to $2n^2 4\pi$ stradians which leads to an extraction efficiency of $1/2n^2$ approximately [26,27]. This simple formula predicts an extraction efficiency of almost 5.5% for semiconductors with refractive index of 3. Such low extraction efficiency is not usually sufficient for laser cooling purposes. There are two main sources of reflection which are responsible for the low extraction efficiency as mentioned earlier: Fresnel reflection and the total internal reflection [28]. Satisfying the boundary conditions of Maxwell's equations necessitates the light refraction and transmission which is described by the Fresnel law for both TE polarization (with the the electric field parallel to the interface) and TM polarization (with the magnetic field parallel to the interface) [29]. It can be infererd from Fresnel law that the reflection increases as the index contrast between the two interface increases. Furthermore as the incident angle deviates from the normal-incidence, the reflection increases up to a point where the reflection reaches 100%. Beyond this critical angle light cannot be transmitted to the outer media and the total internal reflection happens. To have an efficient light extraction from the material both types of aforementioned reflections should be suppressed. In Sections 3.1 and 3.2 we describe effective strategies to reduce the Fresnel and the total internal reflection respectively, and lastly in Section 4, methods to simultaneously supress both reflections are discussed. Two regimes of material dimensions, bulk materials with dimensions much larger than the wavelength of the PL and structures with the dimensions comparable to the wavelength, are discussed separately. The increase in extraction efficiency should not result in material quality degradation, increase in nonradiative recombination rates and the background absorption which reduce the external quantum efficiency [see Eqs. (1)–(3)]. For each luminescence extraction technique, we discuss its advantages and drawbacks (regarding background absorption and nonradiative recombination) and the strategies to optimize it for laser cooling applications.

2. Light extraction of structures with dimensions comparable to wavelength

In this section we describe two important methods to increase the extraction efficiency of the structures with dimensions comparable or smaller than the average wavelength of photoluminesence.

2.1. Subwavelength structures

Making the dimensions of the structure smaller than the photoluminescence (PL) wavelength would result in significant

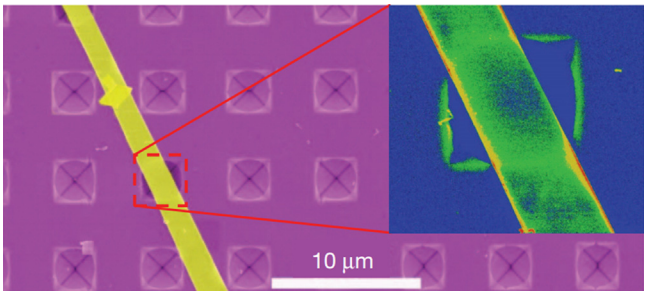

Fig. 2. Light extraction from subwavelength CdS nanobelts. (a) Optical image of the CdS nanobelt. These nanobelts are very thin allowing the PL power to leak out of the active region efficiently. Adapted with permission from Ref. [13].

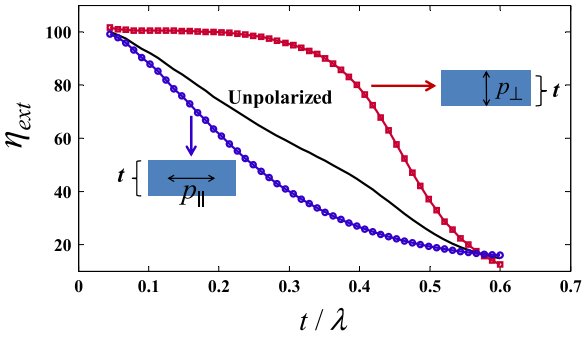

Fig. 3. Simulation of light extraction from a subwavelength structure. The extraction efficiency versus thickness to wavelength ratio (t/λ) for a thin slab. Three different dipole sources were considered with polarization orthogonal (square markers) and parallel (circle markers) to the interface and an unpolarized source. The index of semiconductor (n) is assumed to be 3 and $\lambda=\lambda_0/n$ where λ_0 is the free space wavelength.

enhancement of radiation into far field since the electromagnetic modes in such structures are highly leaky with a very low effective refractive index [30]. A good example of this technique was demonstrated by Zhang et al. [13] for laser cooling of cadmium sulfide (CdS) nanobelts as shown in Fig. 2. The suspended structure is thermally isolated from the substrate and therefore the reabsorption of the rays in the nonsuspended region does not affect the laser cooling of the suspended part. Other optical modes of this thin structure (with the thickness around 100 nm and the emission peak wavelength of 506 nm) which extend to air have very low effective refractive indices and thereby most of their energy is extracted out of the active region. In a recent study, it was shown that the PL reabsorption of such a structure becomes significant if the thickness of the CdS nanobelt becomes more than 120 nm while for thicknesses lower than 65 nm the total absorption of the laser becomes very low and the nonradiative recombination of carriers at the surface states prevails [25]. In general, for any "optically thin structure" there is an optimum thickness for acheiving laser cooling. We have simulated a plain slab which extends to infinity in both of the lateral directions as shown in Fig. 3 using finite difference time domain method (FDTD). A dipole source exists in the middle of the slab to simulate the photoluminesence with dipole orientations parallel and perpendicular to the air/semiconductor interface. We have also simulated the extraction efficiency for an unpolarized dipole source. The thickness of the slab is 300 nm and wavelength span from 1.5 μm to 20 μm. It is evident that as the ratio of the thickness to the wavelength decreases the extraction efficiency increases which is consistent with our expectation. It should be noted that these nanostructures have very low mass and therefore the cooling power in them is very low. For this reason, remedies for light extraction from bulk materials are more important for making practical cryocoolers. Furthermore these nanostructures should be grown without surface imperfections such that surface states do not introduce a challenge.

2.2. Photonic crystals to change the photonic density of states

The use of photonic crystal in thin slabs has been shown to increase the extracted photoluminescence power significantly [31–34]. Special care is needed not to reduce the pump laser absorption due to Bragg reflections using these structures. Furthermore the change of the photonic density of the states may reduce the total radiative decay rate and the quantum effficiency [35].

There are two main approches for using photonic crystals to enhance light extraction from the material: (1) a bandgap approach in which the photonic crystal structure completely penetrates into the active region where the light is emitted. The guided modes that lie within the bandgap radiate into far-field outside the medium efficiently. This method has been investigated both theoretically [35] and experimentally [31,33,36,37], but has two fundamental drawbacks that limit its practical application for laser cooling. First, etching through the active region can potentially increase surface recombination of the carriers that can quickly reach the etched facets and secondly a reduction in the total radiative recombination rate is probable due to the alteration of photonic density of states. (2) A shallower photonic crystal increases the light extraction through the diffraction of guided modes. In this case the guided modes are extracted due to the extra momentum added by the photonic crystal. Careful design of the photonic crystal is needed to completely extract a substantial number of guided modes. In order to effectively couple a guided modes to the air in a 1D photonic crystal, the mode should satisfy the following condition [38]:

$$|k_\parallel + nG| < 2\pi/\lambda \tag{4}$$

where $k_\parallel$ is the in-plane (parallel to the slab surface) wavevector of the mode. n is an interger number and G is the reciprocal lattice vector and is equal to $2\pi/a$ where a is the lattice constant of the photonic crystal and λ is the wavelength of the mode in the free space. The diffracted mode into the free space is a plane wave with the following angle in the far field:

$$\theta = \sin^{-1}[(\lambda/2\pi)|k_\parallel + nG|] \tag{5}$$

Effective 2D photonic crystal can be designed based on the this approach to scatter most of the guided modes out of the material and to enhance the light extraction from 2D slabs. Using this technique a record of extraction efficiency (73%) among unencapsulated GaN Light emitting diodes has been reported [38]. It should be noted that for laser cooling purposes, the effective coupling of the pump laser to the semiconductor slab has to be considered. To achieve this aim, a part of the material should have a photonic crystal that can increase the pump laser considering the laser far-field pattern (for instance: a Gaussian beam for the case of a focused beam near the point of focus) into the active region. As an example a second order grating provides a very high coupling between a single mode fiber and a slab waveguide [39,40]. The energy difference between the pump and the photoluminescence photons (approximately kT) should be considered in all of the designs to have different couplings to different locations inside the active medium for pump and PL light. As pointed out earlier the change in the photonic density of states alters the radiative rate of the emitter and fabrication of these structures may add defects that can lead to the increase in the background absorption or surface recombination rate [37]. While the surface recombination velocity can be reduced by performing surface treatment such as passivation [41], the background absorption can

be prevented by minimzing the implantation of impurities during the fabrication. It is noteworthy to point out that photonic crystals are widely used for optomechanical backaction cooling of specific phonon modes. It has been shown that by using photonic crystals on suspended membranes, cavities that sustain highly confined optical mode with a large coupling to the specific vibrations of the membrane can be realized. These structures have been investigated for optomechanical cooling down to the quantum ground state [42]. These techniques do not lead to microscopic temperature drop as the anti-Stokes mechanism does, but as we proposed previously, they are conceptually relevant to bulk refrigeration and can be tailored to cool down a large number of mechanical modes [8].

3. Light extraction from bulk materials

3.1. Reduction of Fresnel reflection

Fresnel reflection can be suppressed by optical impedence matching either by having a gradual index profile to have an adiabatic coupling from the substrate to air or by employing interferometric effects in stack of layers with quarter wavelength thickness.

3.1.1. Anti-reflective coatings based on destructive interference

This method is based on destructive interference of the reflected light after a round trip in each layer resulting in substantial reduction of the reflected power. The thickness of each layer is equal to one quarter of the wavelength. Since layer thickness is linked to wavelength, therefore it is a very narrowband and a unidirectional method of removing the Fresnel reflection. The total reflection coefficient can be found using the optical matrix of each layer and the transfer matrix method [43–45]. In order to be able to minimize the reflection using available materials with similar refractive indices, sufficient number of layers needs to be deposited which is a practical challenge. Increasing the number of layers can lead to increased defects at the interfaces [46] which can result in unwanted parasitic PL and pump absorption that eventually turns into heat. This is a challenge in addition to its narrowband and unidirectional nature which renders this method unsuitable for laser cooling applications.

3.1.2. Structures with gradually varying refractive index

Fresnel reflection originates from index differences between two different materials. Therefore one straightforward way to reduce Fresnel reflection is to reduce the index difference gradually as envisioned by Lord Rayleigh [47]. Theoretically these structures are broadband as long as the profile of index is distributed over a sufficiently longer length compared to the maximum emission wavelength [48]. There have been many efforts to achieve ideal graded index structures experimentally, having various index profiles including Gaussian, Quintic and exponential [49–51]. In the following we provide the best-reported techniques for either obtaining a direct gradual change of refractive index or by producing a gradual structural change of the high index material in the direction orthogonal to the interface to effectively suppress the Fresnel reflection. Fig. 4 shows our simulations for the transmission of rays inside a semiconductor material ($n=3$) that is covered by a half wavelength thick ($t=\lambda/2=775$ nm) AR coating with linear index profile. These simulations have been performed for transverse electric (TE) and transverse magnetic (TM) polarizations at normal incidence. The gradual index profile is realized by stack of layers that form a step-wise approximation of the linear change of index. As expected, for a larger number of the layers, the transmission is higher but the escape cone does not change. The TM polarized rays can transmit completely to the air at a specific angle within the escape cone. It is evident from Fig. 4 that this particular angle changes by the deposition of the AR coating and eventually in the case of a perfectly linear AR coating the transmission becomes 100% for most of the angles within the escape cone.

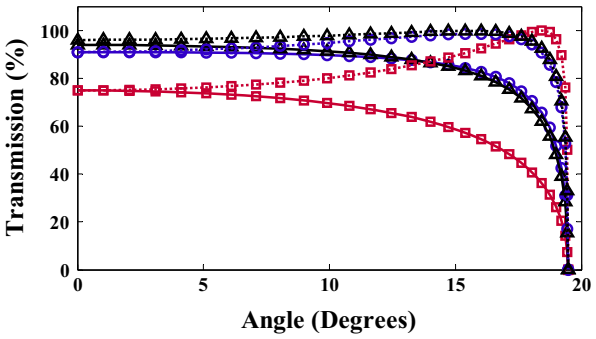

Fig. 4. Simulation of light transmission through graded-index AR coatings. The transmission of the rays from inside of the semiconductor (with index 3) to the outside (air). The interface is covered by a number of layers to make a gradual index profile. The solid (dotted) lines represent the data for TE (TM) polarized rays. Square markers show the graphs for the cases with only one AR layer, while the circles and triangles pertain to AR coatings with two and three layers respectively. Note that the cutoff angle of $\sim 18^\circ$ cannot be changed with the AR coatings, and is only a function of the optical index of the material light starts and ends its path.

Silicon oxynitride (SiO_xN_y) has been extensively used as broadband graded index AR coating for silicon solar cells [52,53]. The change of composition in SiO_xN_y results to refractive index tuning between that of SiO_2 (1.46 at 605 nm) to that of SiN_x ($1.95 < n < 2.99$ at 605 nm) [54]. Silicon oxynitride can be deposited using plasma enhanced vapor phase deposition (PECVD) [55] and low pressure chemical vapor deposition (LPCVD) [56]. For the PECVD deposition, silane gas (SiH_4) acts as silicon precursor with oxygen and nitrogen gases as reactants. Since the reactivity of the oxygen with the silane gas is very high, a small fluctuation of oxygen gas flow results in a considerable change of composition [57]. Mondreanu et al. [58] has calibrated the composition of SiO_xN_y by the gas flow rate of the NH_3 and N_2O and also the platen temperature in a low pressure (LPCVD) chamber.

Another technique to reduce the refractive index of a material is to make it porous. If the pores are much smaller than the wavelength of the light, the medium can be regarded homogenous with an effective refractive index. The optical properties of porous materials can be studied using Bruggeman's effective medium approximation [59]. Making porous materials for the purpose of anti-reflection coating was demonstrated by many groups particularly for the solar cell application. Porous silicon can be fabricated by performing electrochemical etching with hydrofluoric acid [60], spark processing [61] and vapor phase etching [62]. In addition spin coating of porous polymers [63] and deposition of porous SiO_2 [64–67] has been used for the purpose of suppressing the Fresnel reflection. It is important to note that dense materials do not possess a refractive index lower than 1.2. This poses a challenge for gradually changing the refractive index to air. There are many proposed techniques for making porous and low refractive index dielectrics such as chemical etch–leach process on a glass surface [68–70] and sol–gel process [71], evaporative cooling during spin coating [72] and the use of oblique angle deposition [73]. By using an optimized three-layer coating Chajed et al. [64] could obtain a broadband and omni-directional AR coating, reducing the average reflection over angle and wavelength (from 400 nm to 1100 nm) by 42.9%. This type of anti-reflection coatings only has a good potential to be used for laser refrigeration purposes if the problem of total internal reflection is

addressed using other suitable techniques. In addition the background absorption (α_b) in the deposited materials should be completely characterized for the pump and PL wavelength.

Moth-eye AR coatings, which are basically arrays of small protuberances covering the surface, can be used to increase the extraction efficiency based on the concept of graded index AR coating. Wilson and Hutley showed that if the distance between these protuberances is smaller than half of the wavelength of the light in the high index medium and their height is larger than half of the free space wavelength, then they can effectively reduce the Fresnel reflection [74]. This is because from the very top surface of the structure to the bulk of the substrate the amount of the high index material in each cross section increases which in turn increases the effective refractive index of the optical mode propagating into the structure as predicted by the effective medium theory [75]. For semiconductors various techniques have been used to make these protuberances. These include etching techniques and also methods for formation of the mesa using self-assembly of another material. Here we present the most important approaches that have been used in the past for fabrication of these structures. Lastly, we explain the effect of dry etching on the side wall quality and its effect on surface recombination which critically affects the optical refrigeration.

3.1.3. Techniques based on dry etching

In this section, we introduce the most effective methods of employing dry etching to fabricate structures that can increase the extraction efficiency. As we explain later in Section 3.1.4, dry etching is associated with surface damage and the increase in surface recombination velocity that needs to be addressed appropriately when applying any of these methods.

Many of these techniques rely on reactive ion etching with specific recipes that leave behind randomly distributed by products as the etching continues. These by-products act as an effective mask leading to a dense subwavelength textured surface after the subsequent dry etching with a different recipe [76–78]. Depending on the geometry and aspect ratio, these structures can act as an anti-reflection coating for a broad range of wavelengths. One of the best examples of these structures is shown in Fig. 5. The long grass of nanotips were formed on the surface of a crystalline silicon using high-density electron cyclotron resonance (ECR) plasma etching using reactive gases comprising silane (SiH_4), methane (CH_4), hydrogen (H_2) and argon (Ar) [79–81]. Within the general framework of the described method, some alterations are possible. For example: a silicon dioxide layer can be deposited before the first RIE as suggested in Ref. [82] to have a better control over the periodicity and the geometry of the nano-islands or by using femto second lasers [83,84]. By optimization of this technique, extraordinary aspect ratio of the silicon nanotips was obtained by Huang et al. [76] (with the apex diameter in the range of 3–5 nm, a base diameter 200 nm and lengths from 1000 to 16,000 nm, and a nanotip density of 6×10^9 cm^2). Subsequent measurements showed a significant suppression of reflection within a wide angle and spectral range (from UV to THz) as shown in Fig. 6. Although these techniques are quite effective, the RIE recipes are specific for any specific materials system. Similar techniques can be applied to III–V and II–VI highly luminescent materials [85,86]. However most of the recipes were developed for silicon solar cells and unfortunately silicon is not the material of the choice for anti-Stokes laser cooling because it has an indirect bandgap and low internal quantum efficiency (equal to external quantum efficiency when the extraction efficiency is 100%). It should be noted that there is another approach for laser cooling which has been applied to silicon and is based on the increase of the thermal emissivity after the generation of carriers [87,88]. This technique results in a net extraction of energy from the material through blackbody radiation [74,75]. But even in this case, the nonradiative and heat producing mechanisms set the limit for the maximum cooling and should be minimized. Therefore the lateral side wall damage and the increase in the surface recombination velocity should be carefully considered.

3.1.4. A note on dry etching and its damage

As pointed out earlier non-radiative recombination mechanisms propose serious challenges for the optical refrigeration of solids. Therefore care should be taken not to increase the non-radiative processes by using techniques that degrade the quality of the material and increase the SRH recombination rate. It has been shown in the past that dry etching can lead to surface damage [89–91]. This effect has been comprehensively studied by Boroditsky et al. [92]. In that study they measured the external quantum efficiency (see Eq. (1)) by referencing the PL power against a Lambertian reflector as proposed by Schnitzer et al. [93]. It was shown that while dry etching yields a much better surface morphology, which is a prerequisite for fabrication of nanoscale patterns, it damages the surface and produces dangling bonds that increase the surface recombination velocity. Therefore, appropriate surface treatment is needed to recover the surface and to eliminate the dangling bonds [94]. In the case of GaN, this has been achieved by using KOH:H_2O (0.04 M) for 5 s [92]. To study the size-dependency of the adverse effect of dry etching on external quantum efficiency, different mesas with varying diameters were fabricated that contain single InGaAs quantum well as shown in Fig. 7(a) and (b) [92]. Fig. 7(c) shows the measured

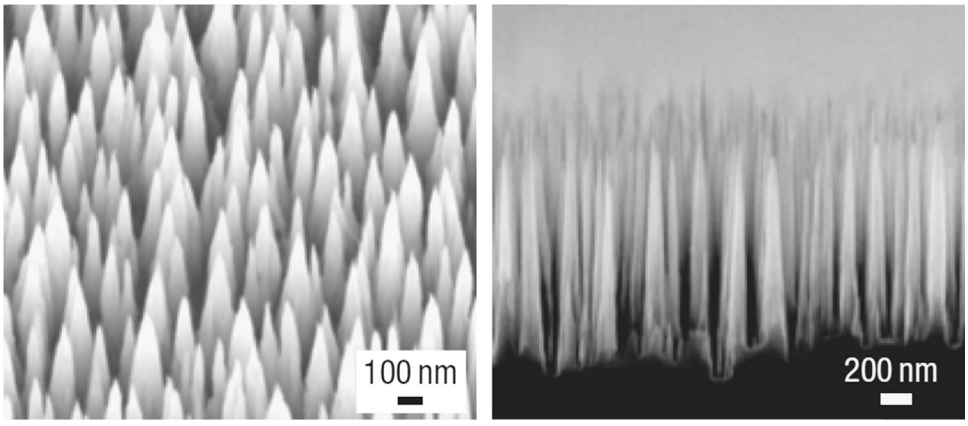

Fig. 5. Image of a moth-eye AR coating fabricated by dry etching. SEM images of the fabricated nanotip grass by a dry etch process showing the apex and the cross-section of them. Adapted with permission from Ref. [76].

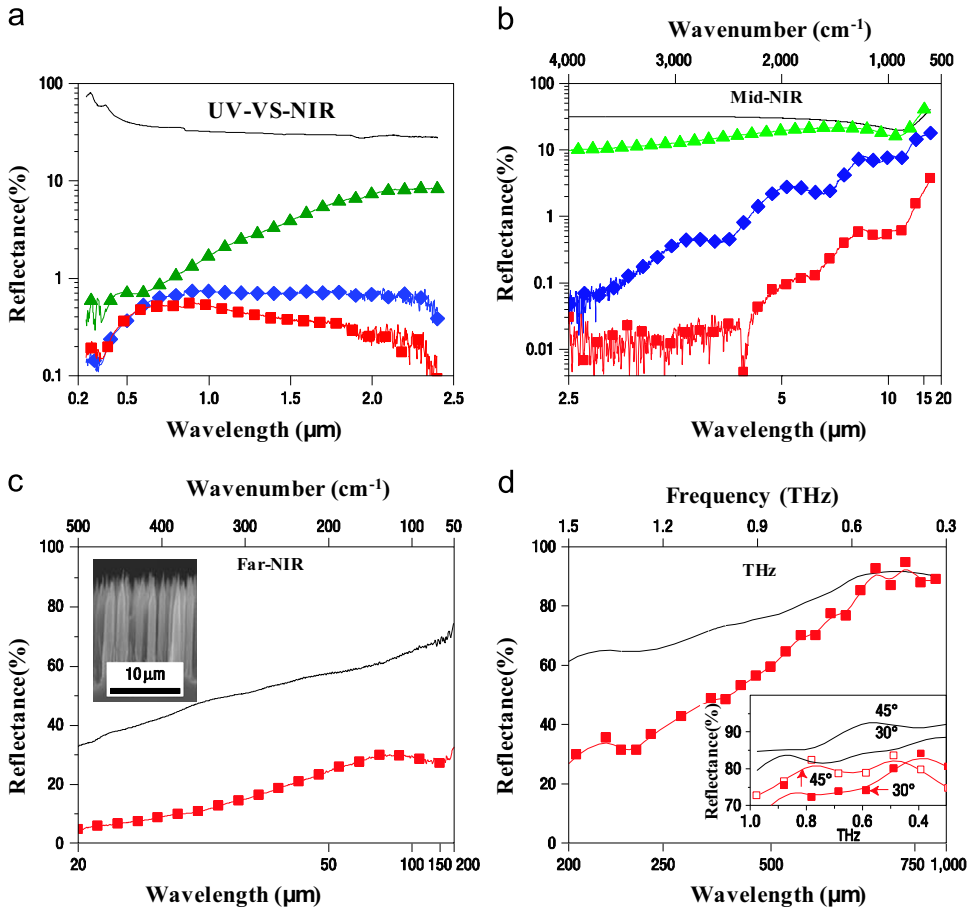

Fig. 6. Reflection data of the moth-eye structure shown in Fig. 5. Hemispherical reflection data obtained using integrated sphere for polished crystalline silicon (black solid lines), silicon nanotips with the length (L) of 1.6 μm (triangular markers), L=5.5 μm (rhombus markers) and L=16 μm (rectangular markers) (a) for the ultraviolet up to near infrared wavelength range, (b) the specular reflectance data for mid-infrared wavelength range, (c) for the far infrared range and (d) for the THz range. The angle of incidence is 30° in all of those specular reflection measurements (b–d). The inset in (c) shows SEM image of the 16 μm long silicon nanotips. The inset in (d) shows the reflectance spectra for angles of incidence of 30 and 45° for polished crystalline silicon (black solid lines) and 16 μm long silicon nanotips (rectangular markers). Adapted with permission from Ref. [76].

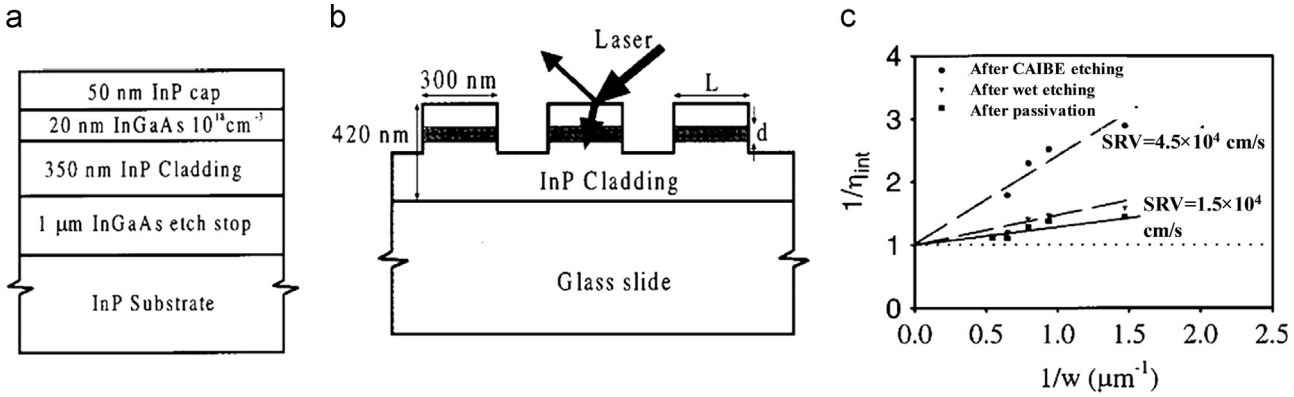

Fig. 7. Effect of dry etching on surface recombination and the internal quantum efficiency. (a) The epilayer structure of the sample under study for the effect of reactive ion etching, (b) the schematics of the fabricated dry etched mesa structures and (c) the inverse of internal quantum efficiency versus the inverse of width of the mesa. The circles are the data after chemically assisted ion beam etching. The triangles are the data after performing a quick wet etching with H_2SO_4:H_2O_2:H_2O 1:8:5000 on the dry etched samples. Subsequent surface passivation with a solution of ammonium sulfide for 5 min made further improvement in internal quantum efficiency as shown by the square markers. The surface recombination velocities (SRV) after the dry etching and after passivation are also shown. Adapted with permission from Ref. [92].

internal quantum efficiency after chemically assisted ion beam etching (dry etching), wet etching and after passivation of the wet etched surfaces. Almost a linear relationship was observed, between the inverse of the external quantum efficiency and the inverse of the diameter of the mesa. Significant suppression of the external quantum efficiency for the dry-etched surfaces is evident. The problem of surface damage was alleviated by performing a brief wet etching (H_2SO_4:H_2O_2:H_2O 1:8:5000) of the $In_{0.53}Ga_{0.47}As$ layer and further improvement was achieved by performing passivation using the ammonium sulfide solution as shown in Fig. 7(c). It is noteworthy to mention that the surface quality degradation by the dry etching depends strongly on the etch depth

and whether it reaches the active epilayer. Therefore a barrier layer to prevent the carriers from reaching the surface is necessary [9,95]. It has been reported that when the etching penetrates the active region, a significant drop of PL intensity is observed because the carriers do not face any barrier to reach the damaged surface [92]. Unfortunately, because of the undercut, the wet etching of semiconductors is not usually compatible with fabrication of ultrafine nanostructures. Therefore appropriate strategies (such as surface treatment and inclusion of a barrier layer) have to be applied to address the challenges of the dry etching and to have a good compromise between the accuracy of fabrication and the increase in surface recombination velocity.

3.1.5. Techniques based on wet etching

These techniques rely on using acids or bases to modify the surface. Wet etching is expected to produce less side wall damage and can be even used in some cases to alleviate the damages of the surface (for instance damages caused by dry etching [89,92]).

Anisotropic wet etching can result in faceted micro- and nanostructures that can reduce the reflections. The surface texturing by this method can be accomplished either through randomly distributed catalyst-assisted wet etching [96] or irregular etch masks [97]. Sun et al. [98] spin-coated monolayer colloidal silica particles and used them as a shadow mask for evaporation of chromium layer. After lifting up the silica particles, nanoholes are formed on the metal surface. Through these nanoholes, KOH solution can etch the silicon substrate anisotropically, leading to inverted pyramid arrays with a normal incidence reflection of almost 10%. Another approach is to coat a large area of self-assembled monolayers consisting of octadecyltrichlorosilane islands that can be used as etch mask for KOH [97]. Such techniques can be used for wet etching of active III–V and II–VI photonic materials as well which are the main candidates for semiconductor laser cooling. As an example, for InP substrates, instead of KOH, HCl-based solutions should be used as highly-anisotropic etchant for InP based compositions [99] and a proper mask should be chosen to resist the etchant without introducing surface damage or unwanted background absorption of the pump and PL.

It should be noted that one of the ways of producing porous surface is by electrochemical wet etching. This method is based on simultaneous agitation of the etching solution by applying electrical current to the electrolyte-containing the etchant [100–102]. Usually the material to be etched is the anode and valence band holes are required for anodized oxidation and subsequent etching [103]. In practice, a large enough positive voltage should be applied such that the electrons tunnel from the valence band to the conduction band leaving behind holes. The tunneling and the etching rate are highly sensitive to the state of the surface. Therefore crystallographic defects and surface impurities which affect the state of the surface are responsible for the resulting porous structures after etching. This technique has been applied to a broad range of materials such as silicon [104], germanium [105], gallium phosphide [103], gallium arsenide [106], and gallium nitride [107] and has been further developed by using light sources (especially UV light) with a technique called photo-assisted electrochemical etching [108]. The reported PL power of the porous InP is approximately 70 percent of the unetched InP prior to etching which indicates that the surface damage is not significant [109]. It is concluded that this method has a potential for laser cooling applications compared to methods that rely on dry etching. However due to the presence of the electrode and accessories to regulate the current, it might not be suitable for mass production [110]. We note that this technique has been used to make efficient antireflection coatings for silicon substrates, but to the best of our knowledge its anti-reflective properties for other materials have not been investigated yet.

3.1.6. Techniques based on self-assembly of organic and inorganic structures

Self-assembly of the subwavelength structures is a simple low cost and scalable technology with minimal damage to the surface of the structure. The self-assembly can be achieved by using either organic or inorganic materials. Inorganic materials possess larger refractive indices and are preferred for laser cooling of semiconductors. Some of the self-assembly techniques are used to form a suitable mask for the subsequent etching to make AR structures. For instance the self-assembly of the octadecyltrichlorosilane islands as described in Section 3.1.5 is used to form etch mask for the wet etching. Another important technique is based on large area self-assembly of microspheres that can be used to transfer nano-patterns to a photoresist layer underneath by exposing to UV light [111–115]. Similar to methods based on dry etching, this method also has a high throughput. It is material independent because the patterns are transferred to photoresist. After the pattern transfer in the photoresist both wet and dry etch can be used to fabricate efficient AR structures. This is a major advantage compared to the dry etching methods that must be optimized for each material individually.

A good example of the self-assembly of the inorganic materials is the precipitation of Ca_2CO_3. For achieving this aim, a saturated $Ca(OH)_2$ is prepared in a solution and then exposed to CO_2 in the ambient which forms Ca_2CO_3 half spheres with micro-scale dimensions [116]. This structure has shown excellent antireflection properties but it requires an equipped chamber and optimized processing conditions for CO_2 flow and temperature. Since it does not require etching, the surface damage is not expected. However the absorption spectrum of $CaCO_3$ should be considered to prevent the unwanted parasitic absorption. Other important self-assembly techniques for realizing AR coating include layer by layer deposition of oppositely charged nanoparticles for tuning the refractive index [117–119] and deposition of colloidal particles by either Langmuir–Blodgett [120] or spin-coating techniques [63,121–123]. In this regard we note that the use of microspheres to increase the extraction efficiency is quite appealing for laser cooling applications. This is due to their low cost, and large availability in the market with a broad range of diameters and the refractive index. Zhu et al. [124] have shown that the extraction efficiency of the GaN diodes can be increased by more than two times using Anatase TiO_2 microspheres with the refractive index of 2.5. This method does not require etching and is thus immune from damages produced during the etching process. However the enhancement in extraction efficiency is not as significant as other methods. The light absorption in the micro-spheres and the impurities introduced during the deposition process is also critical and must be addressed before any method of colloidal particle deposition can be applied to laser cooling.

3.1.7. Growing porous structures

In this method, growth parameters such as the growth rate and temperature are optimized in order to texture the surface and suppress the Fresnel reflection. It has been shown that during the InGaN growth, decreasing the temperature of the wafer results in an increase in the roughness of the surface, which leads to an increase in the light transmission and an enhancement of the performance of the fabricated solar cell [125]. It should be noted that this method is based on the generation of the defect during growth, which can significantly increase the SRH recombination rate. To use this technique for optical refrigeration, the porous material should be the last grown material on the surface and should have a higher bandgap compared to the active region and a barrier layer is also needed to prevent the carriers from reaching the defective porous material where they recombine non-radiatively.

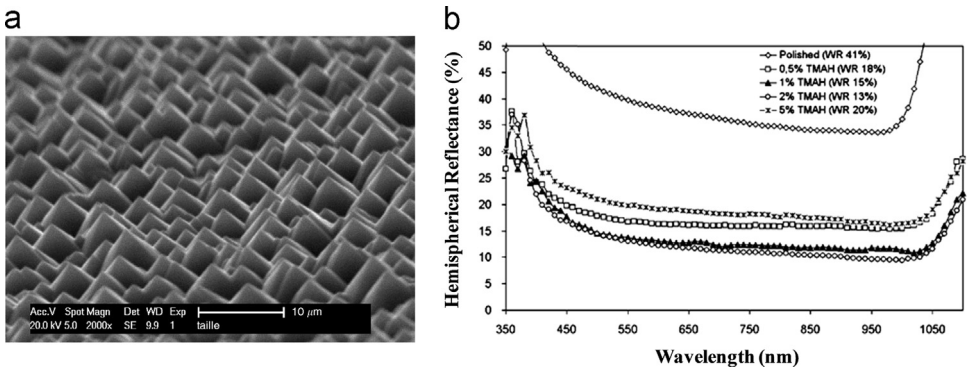

Fig. 8. The use of wet etching to make large structures on the surface for reducing the total internal reflection. SEM image of a wafer after etching 20 min with ultrasonics and 10 min without agitation. The KOH solution contained 2% tetra methyl ammonium hydroxide (TMAH) and 10% isopropyl alcohol. The etching was performed at 80 °C, (b) the hemispherical reflectance of sample etched with different solutions with different TAH concentrations (texturing conditions: 20 min ultrasonics + 10 min without agitation, 10% IPA, 80 °C). It is evident that after etching with 2% TMAH, the weighted reflectance (WR) reduces from 41 to 13%. The illumination source used for this experiment was AM1.5D. Adapted with permission from Ref. [126].

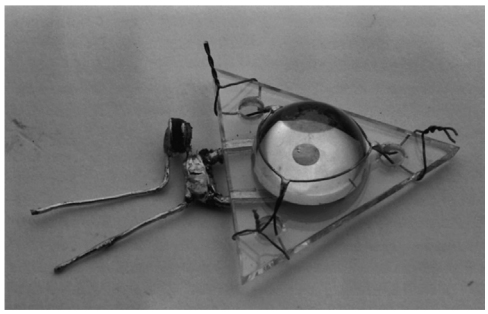

Fig. 9. The use of dome-lens to reduce total internal reflection. A photograph of the dome lens attached to the highly luminescent heterostructure to reduce total internal reflection.

3.2. Reduction of total internal reflection

Large surface structures increase the probability of the rays hitting the interface with angles below the critical angle after a few reflections. In order to make those structures, simple techniques such as standard lithography can be used. In addition, the presence of non-ionic surfactants as shown in Fig. 8 within the wet etchant can result in the formation of very large pyramids after wet etching [126]. It has been also demonstrated that the electrochemical etching of silicon leads to the formation of large mesas [100].

To completely suppress the total internal reflection, each ray inside the material should hit the interface orthogonally. Assuming spherical PL wave propagation at distances far from the luminescent region, attachment of a dome-shaped lens would guarantee orthogonal PL incidence on the lens/air interface. This idea was implemented experimentally both for light emitting diodes [127] and the optical refrigeration. Fig. 9 shows that a GaAs/GaInP heterostructure was attached to a ZnSe dome lens. The ZnSe hemisphere has a relatively large refractive index of 2.5 and negligible background absorption [128]. The ZnSe hemisphere was coated by a broadband (near the wavelength of the photoluminescence) anitireflection coating, ensuring that the transmitted light into the hemisphere does not bounce back by the Fresnel reflection. With the presence of a dome lens, an increase of the external quantum efficiency from 90% to 96% has been reported [129]. The main criteria for the dome lens material are a very low parastic absorption and a refractive index that is close to that of the active region. Proper optical connection of the active region to the dome lens without damaging the surface is also challenging. The final cost and the large size of the final device are shortcomings that prevent its usage in a large scale and for compact cryocooling applications. Furthermore, the large thermal mass of the dome lens lowers the cooling rate [130,131].

4. Methods to reduce both Fresnel reflection and the total internal reflection

In the previous sections, startegies that lead to suppression of either the Fresnel reflection or the total internal reflection were discussed. Here, methods that can simultaneously reduce both types of the reflections, and therefore result in an effective reduction of averaged reflection over angle and wavelength, will be described.

4.1. Combined super-wavelength and sub-wavelength structures

As described in previous section large mesas (compared to the wavelength of light) provide a platform to increase the probability of rays to hit the surface within the escape cone after a few reflections. On the other hand, subwavelength structures effectively act as graded index broadband AR coatings that reduce the Fresnel reflection. Therefore it is expected that the combination of both ideas lead to efficient Ar coatings with enhanced extraction efficiency [132]. Song et al. [28] have fabricated such a structure by first patterning microstructures with standard optical lithography. Subsequent roughening of the mesas was achieved by using silver nanolands as etching mask for dry etching and then removing the silver nanoparticles. As shown in Fig. 10(a), the height and average distance between sub-wavelength nanocones were approximately 120 nm and 150 nm respectively, which were proven optimal for the red LED made of AlGaInP. Fig. 10(b) shows the results of the total transmittance of the scattered light from backside of the sample for subwavelength cones, microstructures and the combined subwavelength structures on the microstructures. A clear improvement of the transmission for the combined structure is observed as shown in Fig. 10(b).

4.2. Fabrication of periodic array of Mie scatterers

Semiconductor structures can possess Mie scattering resonances for wavelengths significantly larger than the structure dimensions [133]. Based on this principle an efficient absorption in silicon nanowire solar cells has been shown [134]. Recently, improved anti-reflection properties of periodic arrays of low-aspect ratio semiconductor cylinder structures have been demonstrated as shown in Fig. 11 [135]. To have a better

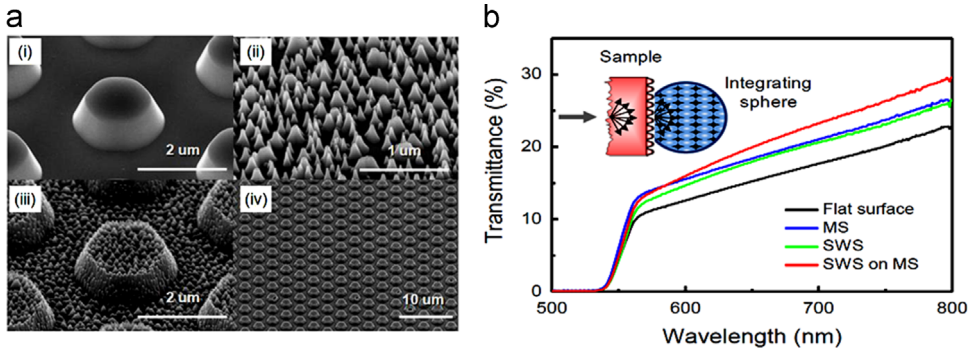

Fig. 10. Combined super-wavelength and sub-wavelength structures to reduce both Fresnel and total internal reflections. (a) Tilted-angle view of SEM images for the fabricated samples with (i) microstructures (MS), (ii) subwavelength structures (SWS), (iii) subwavelength structures fabricated on large mesas on a GaP substrate, and (iv) a lower magnification image of the surface. (b) The transmittance of the fabricated structures. To perform this test the backside of the sample was roughened to produce randomly diffused light (similar to PL for laser cooling applications). The total transmittance was measured using an integrating sphere. Adapted with permission from Ref. [28].

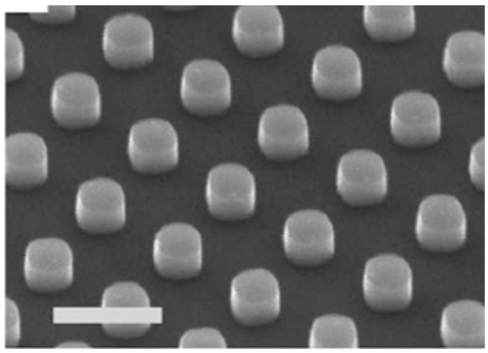

Fig. 11. Image of the array of Mie scatterers that reduce the total reflection. (a) SEM image of the array of semiconductor Mie scatterers (scale bar corresponds to 500 nm). Adapted with permission from Ref. [135].

understanding of this method, three configurations were considered for simulations as shown in Fig. 12: a silicon sphere in air, silicon sphere on a semiconductor substrate, and a silicon cylinder on silicon substrate [135]. Fig. 12(a) shows the calculated scattering cross sections using the FDTD method. For all of these structures, peaks in resonances are identified and assigned to Mie modes. Each Mie scattering mode is a cavity mode that is confined within the semiconductor structure with a quality factor that is limited by radiative loss of the structure. Mie scattering resonance for the silicon cylinder placed on the substrate is comparatively broad and that is because a significant portion of the power of the resonance mode lies in the semiconductor underneath rather than being confined in the cavity. This means that there is a strong coupling between the silicon cylinder and the substrate and light can couple to the substrate through forward Mie scattering with the cylinder [135]. This fact is inferred from the electric field intensity distributions shown in Fig. 12(b–g). Simulations have been performed to optimize the array of these sub-wavelength scatters to reduce the reflection efficiently. Fig. 13 shows that over the entire spectral range from 400 to 1100 nm the reflectivity can be reduced down to $<2\%$ (with exception of a small peak around 650 nm) using these structures. Interestingly the size of nanostructure is small compared to wavelength (250 nm diameter, 150 nm height, 450 nm pitch) and the surface coverage is low (about 30%) but the forward scattering is significant enough, due to the Mie resonance, to enhance the transmission significantly. The sub-wavelength dimensions of this structure, (especially the low height) allow fabricating them by dry etching without reaching the active region. Therefore, as explained before, even a thin barrier layer can be used to prevent the surface recombination at the dry etched surfaces. For these reasons, we believe that this technique is quite advantageous for laser cooling of semiconductors.

Metal particles can as well enhance the light extraction by the forward Mie scattering [136–139]. There are many techniques to produce metallic structures as scattering centers on the surface such as dipping into a solution containing metal particles [140,141], lift off [142] and electro-deposition [143–145]. A very simple and cost effective technique is based on poor adhesion of noble metals such as gold or silver to the dielectric surface. In this method a dielectric layer (the commonly used layers are PECVD silicon dioxide and silicon nitride) is deposited on the surface. Then a thin layer of gold or silver is deposited on the surface of the dielectric. This layer has poor adhesion to the surface and upon annealing, it shrinks and forms nano-islands that can serve as efficient scattering centers. The structures are randomly oriented with no particular exact shape and size. However the average dimensions of the nano-islands are determined by the annealing time and the original metal thickness. The critical drawback is the absorption loss of the metal particles, which results in unwanted heating upon PL absorption. The plasmonic metal loss has been measured by various groups with different techniques such as near field microscopy [146], thermoreflectance [147] and polarization fluorescence anisotropy [148,149]. In addition to the PL absorption in the metal, the system should be designed such that the pump laser does not suffer from the scattering of the nanoparticles. Consequently, a portion of the sample's surface should be allocated for the efficient coupling of the pump laser to the active region as shown in Fig. 14. The PL absorption by the metal nanoparticles reduces the total cooling efficiency according to Eqs. (2) and (3) by increasing the effective background absorption. A systematic study regarding the effect of the dimensions of the metal particles on the light transmission into a high index material has been performed by Ref. [150].

In this regard it has been found that when the wavelength of the light is longer than the particle's resonance, there is enhanced transmission due to the Mie scattering as described before. When the wavelength is close to the nanoparticles' resonance, then the enhanced near-field results in an efficient energy transfer to the high index material. For wavelengths much smaller than the resonance the transmission is lower due to the destructive interference between the scattered and un-scattered electromagnetic waves which is known as the Fano effect. Laser cooling at longer wavelengths can be benefited by this method because the loss of the metal particles becomes negligible for photon frequencies much lower than the plasma frequency of the metal.

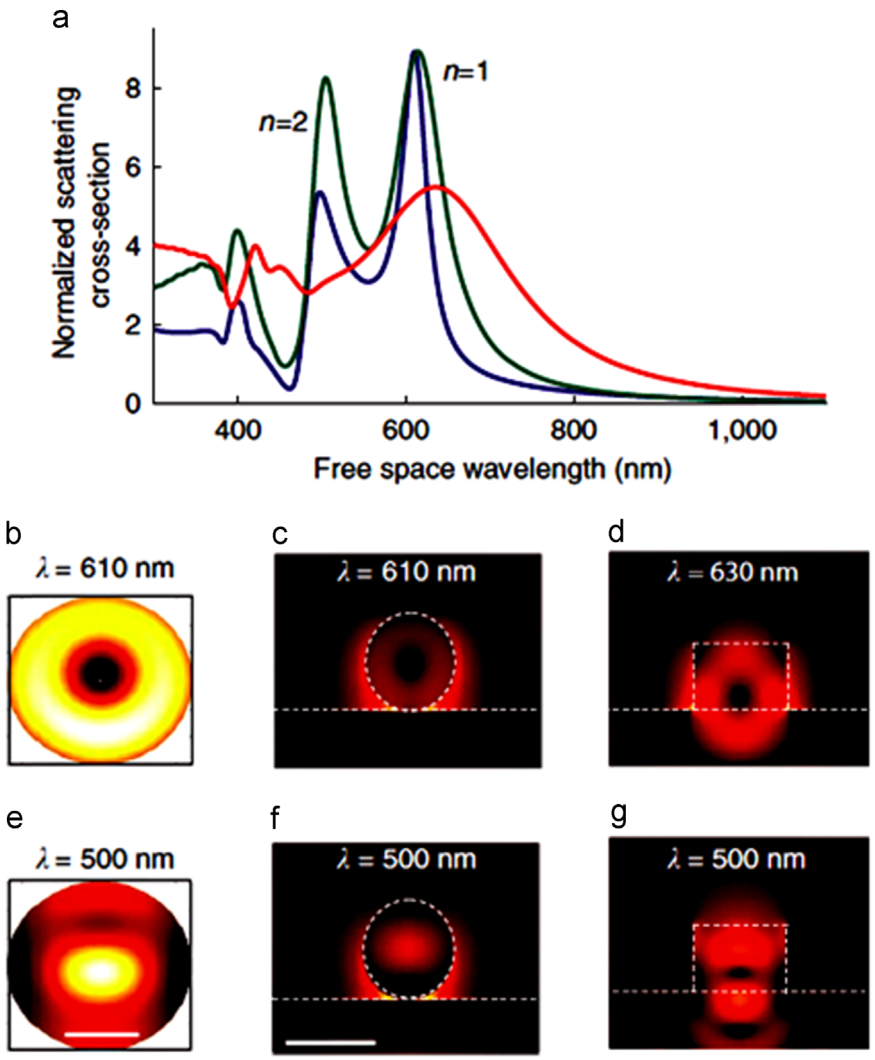

Fig. 12. Simulation of Mie scattering to understand its anti-reflective properties. Scattering cross section versus wavelength for a silicon sphere (blue), a silicon sphere on a silicon substrate (green) and a silicon cylinder on a silicon substrate (red). The first and second Mie resonances are also indicated (b–g). Electric field intensity profile of three different configurations for the first and second Mie resonance wavelengths (610 nm and 500 nm): (b,e) a silicon sphere in air, (c,f) a silicon sphere on a silicon substrate and (d,g) a sphere cylinder, with the geometry similar to Fig. 11, on a silicon substrate. In all of the above simulations the sphere has a diameter of 150 nm and the cylinder has an in-plane diameter of 150 nm and height of 100 nm. Adapted with permission from Ref. [135]. (For interpretation of the references to color in this figure legend, the reader is referred to the web version of this article.)

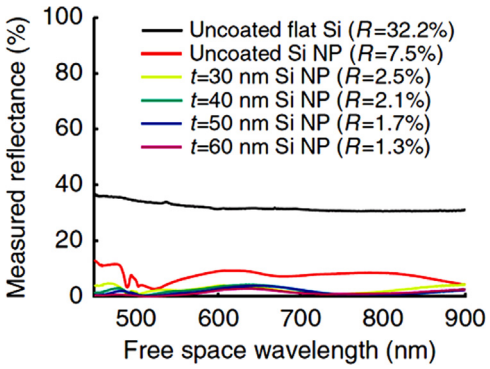

Fig. 13. Comparison of the surface reflectivity with and witout Mie scatterers. The total reflectivity of: bare silicon wafer and silicon Mie scatterer arrays [denoted as silicon nanoparticles (NPs)] with and without silicon nitride with different thicknesses denoted by t (colors). The cylindrical Mie scatterers have a diameter of 125 nm, height of 150 nm and a spacing of 450 nm. For each structure the average reflectivity, R weighted with the AM1.5 solar spectrum, is indicated. The presence of the Mie scatterers reduces the reflectance significantly. Adapted with permission from Ref. [135]. (For interpretation of the references to color in this figure legend, the reader is referred to the web version of this article.)

4.3. Evanescent coupling of the photoluminescence

Light reflection inside the semiconductor is associated with an evanescent wave at other side of the interface. Therefore if another medium with approximately the same refractive index comes within the decay length of the evanescent mode of the luminescent medium, there will be efficient electromagnetic energy transfer between the two (see Fig. 15). In this case the presence of the vacuum gap (which is usually less than 100 nm) ensures a good thermal isolation such that the absorption of the PL in the second medium would not affect the cooling of the active region. Martin et al. [130] have investigated the realization of this technique by first thermally growing 100 nm of silicon dioxide on a crystalline silicon wafer. By performing electron beam lithography nanoholes were defined in the silicon dioxide release layer. Then a layer of amorphous silicon was deposited on the top of the patterned silicon dioxide. After sacrificial etchings of the silicon dioxide layer using the buffered oxide etch, suspended amorphous silicon layer is formed and supported by nano-posts. Temperature measurements of the areas with the nanogap proved that the thermal isolation between the crystalline and amorphous silicon is

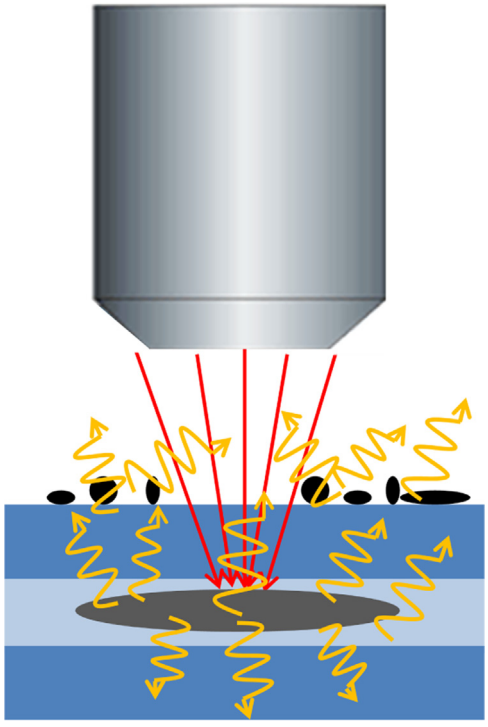

Fig. 14. The use of metal particles to enhance light extraction for optical refrigeration). The scattering by silver nanoparticles increases the extraction efficiency. However a region on the surface should be allocated for pumping the material without having the silver nanoparticles. The generated carriers are confined by the barrier layers in the vertical direction, but in the lateral directions they diffuse. Therefore PL is emitted from a larger area compared to the pump spot size.

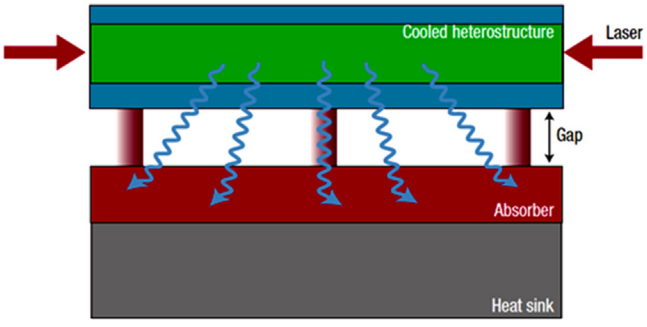

Fig. 15. Illustration of evanescent luminescence extraction. The idea of nanogap for evanescently coupling the PL to another medium while maintaining the thermal isolation. Adapted with permission from Ref. [9]. Realization of this structure has been reported by Ref. [130].

quite satisfactory [130]. However the yield of the fabrication was reported to be low, particularly due to the residual stress of the amorphous silicon that can make it bent and touching the substrate.

Another way of implementing of the evanescent extraction is by the use of surface plasmon polaritons. Consider a metal–semiconductor interface. Based on the Drude theory the dielectric constant of the metal can be negative near the surface plasmon resonance. As the magnitude of the negative refractive index of metal approaches that of the semiconductor a very confined plasmonic mode is formed near the interface. In this situation the plasmonic density of states becomes very high and that facilitates the transfer of optical energy to the plasmonic modes [151]. A similar technique was applied to enhance the luminescence of GaN coated with a thin film of metal [152]. Although the increase in the density of surface plasmons assists the transfer of the energy to the surface plasmon polaritons, the radiation efficiency of the surface plasmons is not high. This is due to the fact that there are electron–electron and phonon–electron interactions that interact within few femto second time scale that lead to the loss of energy and produce heat [153]. Khurgin has proposed that if the energy transferred to surface plasmon polaritons could be taken away from the active region, the aim of the laser cooling would be achieved [151]. Therefore by using a thermal isolation layer in between the metal and the dielectric and by patterning metal to have heat sink, the heat produced by the surface plasmon polaritons can be transferred to the ambient. Although this concept has been theoretically demonstrated, practical implementation of this method has not been shown yet. The difficulty associated with this technique is the residual stress and bowing of the metal that may prevent achieving a uniform nanogap across the sample. Also due to the metal loss, the imaginary component of the dielectric constant results in a different dispersion curve from the ideal case, which reduces the density of states of the plasmonic modes and the energy transfer from the semiconductor to the surface plasmon polaritons [151].

5. Conclusions and perspectives

In summary, we introduced the advantages and the challenges of laser cooling of semiconductors. To improve the cooling efficiency of the anti-Stokes optical refrigeration, the extraction efficiency of the PL emitted by the material should be maximized. The aim of this review was to outline the most effective strategies to increase the PL extraction efficiency and subsequently the external quantum efficiency which is a key parameter of optical refrigeration. These strategies with their advantages, drawbacks and their relative importance for improving the performance of the future optical refrigerators have been summarized in Table 1. They have been also categorized based on material dimensions. Properly designed subwavelength structures and photonic crystals fabricated on structures with dimensions comparable to the wavelength, can significantly increase the light out-coupling. For the case of bulk materials the two sources of reflections namely Fresnel and total internal reflections should be addressed appropriately. Two main approaches of suppressing the Fresnel reflection are the use of interferometric effects of quarter wavelength coatings and the realization of structures with gradual index profiles from the substrate to the host medium (usually air). We discussed the effect of dry etching on the final surfaces and showed that this can lead to unwanted surface recombination that generates heat. Therefore, we provided guidelines to effectively employ dry etching for making accurate subwavelength structures without significantly increasing the surface recombination rate of the photogenerated carriers. Various wet etching and self-assembly formations of AR coating were pointed out. These methods are low-cost and less destructive than dry etching. However, it is more difficult to achieve the ideal geometries with the desired refractive index profile using these methods. The suppression of total internal reflection by fabrication of large microstructures and practical use of a dome lens were explained. Finally, we introduced techniques to suppress both Fresnel and total internal reflections using AR coated dome lens, surface texturing of large mesas, Mie scattering, self-assembly of lens-like structures and evanescent PL coupling. The internal quantum efficiency of the material determines the minimum required extraction efficiency to achieve laser cooling. Therefore, considering the fabrication feasibility and its effect on non-radiative recombinations, proper strategies such as those we discussed in this paper should be applied for realizing future semiconductor optical refrigerators.

Table 1
A summary of the introduced extraction strategies along with their conditions of applicability, advantages, drawbacks and our estimated ratings for their use in laser refrigerators in the next 20 years.

Extraction strategy	Application requirements	Advantages	Drawbacks	Refs.	Expected rating for its use in future optical cryocoolers
Subwavelength structures	The dimensions of the device should be much smaller than the PL wavelength	The extraction efficiency can be very close to the ideal value of 100% for highly leaky optical modes.	1. The laser absorption and the cooling power reduces as the device becomes smaller. 2. The surface recombination velocity becomes more pronounced for smaller devices.	[25]	Excellent for nanostructures
Photonic crystals (bandgap approach)	The active medium is within the photonic crystal	The extraction efficiency can be very close to the ideal value of 100% by proper design of the photonic crystal	1. Etching through active medium may result in damage. Furthermore, the effective surface of the active medium increases (which may lead to more surface recombination). 2. The reduction of photonic density of states can lead to the reduction of the total radiative recombination rate 3. Requires accurate fabrication.	[31,33,35–37]	Poor
Photonic crystals (diffractive approach)	It is implemented on thin slabs of active medium with guided modes	1. The extraction efficiency can be made very high. 2. The photonic crystal does not penetrate into active region and fabrication damages can be prevented.	1. Requires a specific design to maintain a good pump laser coupling to the active region. 2. Requires accurate fabrication.	[38]	Good
Quarter wavelength AR coating	It can be applied only to bulk materials	1. Easy to fabricate with current deposition technologies 2. Significantly reduces the Fresnel reflection for a particular wavelength.	It is spectrally narrowband and does not solve the problem of total internal reflection.	[43–46]	Poor
Gradually varying the refractive index (through material compositional change, porosity, surface texturing, self-assembly of other materials, etc…)	It can be applied to any material as long as it is compatible with fabrication methodology	1. various fabrication techniques, based on the material and the geometry of interest can be employed. 2. It can suppress the Fresnel reflection within a broad range of wavelengths. 3. Low-cost, scalable and large area self-assembly techniques have been developed to make effective AR coatings.	1. This technique by itself cannot address the problem of total internal reflection. 2. Care should be given not to damage the material by applying any of these methods (for instance when dry etching or growing porous materials is used).	[52–54,76–78,116,124]	Excellent (if used in conjunction with techniques that suppress the total internal reflection)
Large mesa structures	It can be applied only to bulk materials	Simple and low cost fabrication methods have been developed to make these structures with minimal damage to the active region	The technique by itself cannot address the problem of Fresnel reflection	[126]	Excellent (if used in conjunction with techniques that suppress the Fresnel reflection)
Dome lens attachment	1. Can be applied only to any material with refractive index close to the dome lens 2. The parasitic absorption of PL should be avoided by choosing the right material for the dome lens	Simple and straightforward technique to eliminate the total internal reflection within a broad range of wavelengths	1. The dome lens is bulky and expensive. 2. Connecting the dome lens to the active material without damage can be challenging. 3. Added thermal mass of the dome lens can slow down the cooling process. 4. Dome lens by itself cannot address the Fresnel reflection.	[127–131]	Good (if used in conjunction with techniques that suppress the Fresnel reflection)
Mie scattering	It can be applied to bulk materials	1. Suppresses both the Fresnel reflection and total internal reflection effectively. 2. Mie scattering can happen by the structures significantly smaller than wavelength and far from the active region. Therefore the deterioration of material quality can be prevented.	For the case of Mie scattering with metal particles, pump and PL absorption in metal particles can lead to unwanted heating	[135–139]	Excellent
Evanescent coupling	It can be applied to bulk materials with low degree of surface roughness	Suppresses both the Fresnel reflection and total internal reflection effectively	Successful fabrication of nanogap while maintaining a high thermal isolation between the PL absorber and the cooling medium is challenging in practice	[9,130,151]	Good

Acknowledgments

We would like to acknowledge the partial support from NSF award #ECCS-131062, DARPA award #W911NF-13-1-0485 and ARO award #W911NF-11-1-0390, as well as the support from high performance computational center (QUEST) at Northwestern University.

References

[1] B. Imangholi, M.P. Hasselbeck, D.A. Bender, C. Wang, M. Sheik-Bahae, R.I. Epstein, S. Kurtz, in: Proceedings of the Society of Photo-optical Instrumentation Engineers (SPIE), vol. 6115, 2006, p. 6115C.
[2] M. Sheik-Bahae, R.I. Epstein, Laser Photonics Rev. 3 (2009) 64.
[3] C. Wang, M.P. Hasselbeck, C.-Y. Li, M. Sheik-Bahae, in: Proceedings of the Society of Photo-optical Instrumentation Engineers (SPIE), vol. 7614, 2010, p. 76140B.
[4] B. Imangholi, C. Wang, E. Soto, M. Sheik-Bahae, A. Stintz, K. Malloy, N. Nuntawong, R. Epstein, in: Proceedings of the Society of Photo-optical Instrumentation Engineers (SPIE), vol. 6461, 2007, p. 64610G.
[5] C. Wang, C.-Y. Li, M.P. Hasselbeck, T. Rotter, K. Malloy, M. Sheik-Bahae, J. Olson, in: Proceedings of the Society of Photo-optical Instrumentation Engineers (SPIE), vol. 7951, 2011, p. 79510D.
[6] S. Melgaard, A.R. Albrecht, M. Hehlen, D. Seletskiy, M. Sheik-Bahae, Optical refrigeration cools below 100K, in: CLEO: QELS_Fundamental Science. Optical Society of America, 2014, p. FTh4D. 4.
[7] R.I. Epstein, M.P. Hehlen, M. Sheik-Bahae, S.D. Melgaard, in: Proceedings of the Society of Photo-optical Instrumentation Engineers (SPIE), vol. 9070, 2014, p. 90702k.
[8] I.H. Nia, H. Mohseni, Appl. Phys. Lett. 105 (2014) 042102.
[9] M. Sheik-Bahae, R.I. Epstein, Nat. Photonics 1 (2007) 693.
[10] V. Malyutenko, V. Bogatyrenko, O.Y. Malyutenko, J. Appl. Phys. 108 (2010) 073104.
[11] G. Nemova, R. Kashyap, Phys. Rev. A 83 (2011) 013404.
[12] J. Clark, G. Rumbles, Phys. Rev. Lett. 76 (1996) 2037.
[13] J. Zhang, D. Li, R. Chen, Q. Xiong, Nature 493 (2013) 504.
[14] M. Ghasemkhani, A.R. Albrecht, S.D. Melgaard, D.V. Seletskiy, J.G. Cedeberg, M. Sheik-Bahae, in: Proceedings of the Society of Photo-optical Instrumentation Engineers (SPIE), vol. 9380, 2015, p. 938003.
[15] G. Nemova, R. Kashyap, Rep. Prog. Phys. 73 (2010) 086501.
[16] G. Nemova, R. Kashyap, J. Opt. Soc. Am. B 29 (2012) 676.
[17] G. Nemova, R. Kashyap, J. Opt. Soc. Am. B 29 (2012) 3034.
[18] G. Nemova, R. Kashyap, in: Proceedings of the Society of Photo-optical Instrumentation Engineers (SPIE), vol. 8915, 2013, p. 89151T.
[19] R.I. Epstein, M.I. Buchwald, B.C. Edwards, T.R. Gosnell, C.E. Mungan, Nature 377 (1995) 500.
[20] R. Epstein, M. Sheik-Bahae, Optical Refrigeration: Science and Applications of Laser Cooling of Solids, Wiley, 2009.
[21] M. Sheik-Bahae, R.I. Epstein, Phys. Rev. Lett. 92 (2004) 247403.1.
[22] C. Wang, C.-Y. Li, M.P. Hasselbeck, B. Imangholi, M. Sheik-Bahae, J. Appl. Phys. 109 (2011) 093108.
[23] M. Sheik-Bahae, B. Imangholi, M. Hasselbeck, R. Epstein, S. Kurtz, in: Proceedings of the Society of Photo-optical Instrumentation Engineers (SPIE), vol. 6115, 2006, p. 611518B.
[24] P.K. Basu, Theory of Optical Processes in Semiconductors: Bulk and Microstructures, Oxford University Press, 1997.
[25] D. Li, J. Zhang, Q. Xiong, Opt. Exp. 21 (2013) 19302.
[26] N.C. Greenham, R.H. Friend, D.D. Bradley, Adv. Mater. 6 (1994) 491.
[27] J. Lee, N. Chopra, F. So, Appl. Phys. Lett. 92 (2008) 033303.
[28] Y.M. Song, G.C. Park, S.J. Jang, J.H. Ha, J.S. Yu, Y.T. Lee, Opt. Exp. 19 (2011) A157.
[29] M.C. Teich, B. Saleh, Fundamentals of Photonics, Wiley Intersci., Canada, 1991.
[30] W.N. Wang, P.A. Shields, C. Liu, D.W. Allsopp, F. Causa, Advances in nano-enabled GaN photonic devices, in: Proceedings of the Society of Photo-optical Instrumentation Engineers (SPIE), vol. 7945, 2011, p. 794523.
[31] M. Boroditsky, T. Krauss, R. Coccioli, R. Vrijen, R. Bhat, E. Yablonovitch, Appl. Phys. Lett. 75 (1999) 1036.
[32] E. Matioli, E. Rangel, M. Iza, B. Fleury, N. Pfaff, J. Speck, E. Hu, C. Weisbuch, Appl. Phys. Lett. 96 (2010) 031108.
[33] J.-Y. Kim, M.-K. Kwon, S.-J. Park, S.H. Kim, K.-D. Lee, Appl. Phys. Lett. 96 (2010) 251103.
[34] E. Matioli, C. Weisbuch, J. Phys. D: Appl. Phys. 43 (2010) 354005.
[35] J.B. Khurgin, J. Appl. Phys. 100 (2006) 113116.
[36] H. Ryu, Y. Lee, R. Sellin, D. Bimberg, Appl. Phys. Lett. 79 (2001) 3573.
[37] M. Fujita, S. Takahashi, Y. Tanaka, T. Asano, S. Noda, Science 308 (2005) 1296.
[38] J.J. Wierer, A. David, M.M. Megens, Nat. Photonics 3 (2009) 163.
[39] D. Taillaert, W. Bogaerts, P. Bienstman, T.F. Krauss, P. Van Daele, I. Moerman, S. Verstuyft, K. De Mesel, R. Baets, IEEE J. Quantum Electron. 38 (2002) 949.
[40] D. Taillaert, F. Van Laere, M. Ayre, W. Bogaerts, D. Van Thourhout, P. Bienstman, R. Baets, Jpn. J. Appl. Phys. 45 (2006) 6071.
[41] D. Englund, H. Altug, J. Vučković, Appl. Phys. Lett. 91 (2007) 071124.
[42] M. Eichenfield, R. Camacho, J. Chan, K.J. Vahala, O. Painter, Nature 459 (2009) 550.
[43] G. Darvish, M.K. Moravvej-Farshi, A. Zarifkar, K. Saghafi, Appl. Opt. 47 (2008) 5140.
[44] Z. Zhao, S. Bouchoule, J. Song, E. Galopin, J.-C. Harmand, J. Decobert, G. Aubin, J.-L. Oudar, Opt. Lett. 36 (2011) 4377.
[45] M. Strain, M. Gnan, G. Bellanca, R. De La Rue, M. Sorel, Opt. Exp. 17 (2009) 13493.
[46] H. Wang, H. Qi, B. Wang, Y. Cui, M. Guo, J. Zhao, Y. Jin, J. Shao, Opt. Exp. 23 (2015) 5213.
[47] L. Rayleigh, Proc. Lond. Math. Soc. 1 (1879) 51.
[48] S.A. Boden, D.M. Bagnall, Appl. Phys. Lett. 93 (2008) 133108.
[49] E. Spiller, I. Hailer, R. Feder, J. Baglin, W. Hammer, Appl. Opt. 19 (1980) 3022.
[50] P. Yeh, S. Sari, Appl. Opt. 22 (1983) 4142.
[51] W.H. Southwell, Opt. Lett. 8 (1983) 584.
[52] V. Aroutiounian, K. Martirosyan, P. Soukiassian, J. Phys. D: Appl. Phys. 39 (2006) 1623.
[53] M. Serenyi, M. Racz, T. Lohner, Vacuum 61 (2001) 245.
[54] M. Lipiński, A. Kaminski, J.F. Lelièvre, M. Lemiti, E. Fourmond, P. Zięba, Phys. Status Solidi C 4 (2007) 1566.
[55] K. Wörhoff, A. Driessen, P. Lambeck, L. Hilderink, P. Linders, T.J. Popma, Sens. Actuators A 74 (1999) 9.
[56] A.E.T. Kuiper, S.W. Koo, F.H.P.M. Habraken, Y. Tamminga, J. Vac. Sci. Technol. J. Vac. Sci. Technol. 1 (1983) 62.
[57] S. Callard, A. Gagnaire, J. Joseph, J. Vac. Sci. Technol. A 15 (1997) 2088.
[58] M. Modreanu, N. Tomozeiu, P. Cosmin, M. Gartner, Thin Solid Films 337 (1999) 82.
[59] D. Bruggeman, Ann. Phys. Leipzig 24 (1935) 636.
[60] X. Li, P. Bohn, Appl. Phys. Lett. 77 (2000) 2572.
[61] M. Saadoun, N. Mliki, H. Kaabi, K. Daoudi, B. Bessaïs, H. Ezzaouia, R. Bennaceur, Thin Solid Films 405 (2002) 29.
[62] R.E. Hummel, S.S. Chang, Appl. Phys. Lett. 61 (1992) 1965.
[63] S. Walheim, E. Schäffer, J. Mlynek, U. Steiner, Science 283 (1999) 520.
[64] S. Chhajed, M.F. Schubert, J.K. Kim, E. Fred Schubert, Appl. Phys. Lett. 93 (2008) 251108.
[65] K. Wongcharee, M. Brungs, R. Chaplin, Y. Hong, R. Pillar, E. Sizgek, J. Sol–Gel Sci. Technol. 25 (2002) 215.
[66] S. Chhajed, D.J. Poxson, X. Yan, J. Cho, E.F. Schubert, R.E. Welser, A.K. Sood, J. K. Kim, Appl. Phys. Exp. 4 (2011) 052503.
[67] B.G. Prevo, Y. Hwang, O.D. Velev, Chem. Mater. 17 (2005) 3642.
[68] M.J. Minot, J. Opt. Soc. Am. (1917–1983) 66 (1976) 515.
[69] Y. Asahara, T. Izumitani, J. Non-Cryst. Solids 42 (1980) 269.
[70] B.E. Yoldas, D.P. Partlow, Appl. Opt. 23 (1984) 1418.
[71] G. Wu, J. Wang, S. Jun, T. Yang, Q. Zhang, B. Zhou, Z. Deng, B. Fan, D. Zhou, F. Zhang, in: Proceedings of the Society of Photo-optical Instrumentation Engineers (SPIE), vol. 4086, 2000, p. 807.
[72] M.S. Park, J.K. Kim, Langmuir 21 (2005) 11404.
[73] J.-Q. Xi, M.F. Schubert, J.K. Kim, E.F. Schubert, M. Chen, S.-Y. Lin, W. Liu, J. A. Smart, Nat. Photonics 1 (2007) 176.
[74] S. Wilson, M. Hutley, J. Mod. Opt. 29 (1982) 993.
[75] J. Dobrowolski, D. Poitras, P. Ma, H. Vakil, M. Acree, Appl. Opt. 41 (2002) 3075.
[76] Y.-F. Huang, S. Chattopadhyay, Y.-J. Jen, C.-Y. Peng, T.-A. Liu, Y.-K. Hsu, C.-L. Pan, H.-C. Lo, C.-H. Hsu, Y.-H. Chang, Nat. Nanotechnol. 2 (2007) 770.
[77] C. Lee, S.Y. Bae, S. Mobasser, H. Manohara, Nano Lett.. 5 (2005) 2438.
[78] J. Yoo, G. Yu, J. Yi, Mater. Sci. Eng. B 159 (2009) 333.
[79] T. Glaser, A. Ihring, W. Morgenroth, N. Seifert, S. Schröter, V. Baier, Microsyst. Technol. 11 (2005) 86.
[80] C.-H. Hsu, H.-C. Lo, C.-F. Chen, C.T. Wu, J.-S. Hwang, D. Das, J. Tsai, L.-C. Chen, K.-H. Chen, Nano Lett. 4 (2004) 471.
[81] K.-H. Chen, J.S. Hwang, D. Das, H.C. Lo, L.-C. Chen, Method of forming a nanotip array in a substrate by forming masks on portions of the substrate and etching the unmasked portions, in: Google Patents, 2005.
[82] M. Schnell, R. Ludemann, S. Schaefer, Plasma surface texturization for multicrystalline silicon solar cells, in: Proceedings of the Conference Record of the Twenty-Eighth IEE Photovoltaic Specialists Conference, 2000, p. 367.
[83] C. Radu, S. Simion, M. Zamfirescu, M. Ulmeanu, M. Enculescu, M. Radoiu, J. Appl. Phys. 110 (2011) 034901.
[84] R. Younkin, J. Carey, E. Mazur, J. Levinson, C. Friend, J. Appl. Phys. 93 (2003) 2626.
[85] X. Chen, Z.-C. Fan, Y. Xu, G.-F. Song, L.-H. Chen, Microelectron. Eng. 88 (2011) 2889.
[86] D.S. Hobbs, B.D. MacLeod, E. Sabatino, S.B. Mirov, D.V. Martyshkin, in: Proceedings of the Society of Photo-optical Instrumentation Engineers (SPIE), vol. 8530, 2012, p. 85300PB.
[87] V. Malyutenko, V. Bogatyrenko, O.Y. Malyutenko, Appl. Phys. Lett. 102 (2013) 241102.
[88] V. Malyutenko, V. Bogatyrenko, O.Y. Malyutenko, in: Proceedings of the Society of Photo-optical Instrumentation Engineers (SPIE), vol. 7606, 2010, p. 760617.
[89] S. Pang, J. Electrochem. Soc. 133 (1986) 784.
[90] S. Pearton, J. Lee, J. MacKenzie, C. Abernathy, R. Shul, Appl. Phys. Lett. 67 (1995) 2329.
[91] S. Pearton, U. Chakrabarti, F. Baiocchi, Appl. Phys. Lett. 55 (1989) 1633.

[92] M. Boroditsky, I. Gontijo, M. Jackson, R. Vrijen, E. Yablonovitch, T. Krauss, C.-C. Cheng, A. Scherer, R. Bhat, M. Krames, J. Appl. Phys. 87 (2000) 3497.
[93] I. Schnitzer, E. Yablonovitch, C. Caneau, T. Gmitter, Appl. Phys. Lett. 62 (1993) 131.
[94] S.-i Gozu, K. Akahane, N. Yamamoto, A. Ueta, N. Ohtani, M. Tsuchiya, J. Vac. Sci. Technol. B 24 (2006) 2291.
[95] B. Imangholi, M.P. Hasselbeck, M. Sheik-Bahae, R.I. Epstein, S. Kurtz, Appl. Phys. Lett. 86 (2005) 081104.
[96] S. Koynov, M.S. Brandt, M. Stutzmann, Appl. Phys. Lett. 88 (2006) 203107.
[97] W.-T. Wang, N. Lu, J.-Y. Hao, H.-B. Xu, D.-P. Qi, L.-F. Chi, J. Phys. Chem. C 114 (2010) 1989.
[98] C.-H. Sun, W.-L. Min, N.C. Linn, P. Jiang, B. Jiang, Appl. Phys. Lett. 91 (2007) 231105.
[99] I.H. Nia, H. Mohseni, ECS Solid State Lett. 2 (2013) P44.
[100] H. Lv, H. Shen, Y. Jiang, C. Gao, H. Zhao, J. Yuan, Appl. Surf. Sci. 258 (2012) 5451.
[101] P. Kleimann, X. Badel, J. Linnros, Appl. Phys. Lett. 86 (2005) 183108.
[102] H. Asoh, K. Sasaki, S. Ono, Electrochem. Commun. 7 (2005) 953.
[103] R. Tjerkstra, J.G. Rivas, D. Vanmaekelbergh, J. Kelly, Electrochem. Solid-state Lett. 5 (2002) G32.
[104] P. Kleimann, J. Linnros, S. Petersson, Mater. Sci. Eng. B 69 (2000) 29.
[105] S. Tutashkonko, A. Boucherif, T. Nychyporuk, A. Kaminski-Cachopo, R. Arès, M. Lemiti, V. Aimez, Electrochim. Acta 88 (2013) 256.
[106] J. Sabatairyt, I. Šimkien, R.-A. Bendorius, K. Grigoras, V. Jasutis, V. Pačebutas, H. Tvardauskas, K. Naudžius, Mater. Sci. Eng. C 19 (2002) 155.
[107] G. Nowak, X. Xia, J. Kelly, J. Weyher, S. Porowski, J. Cryst. Growth 222 (2001) 735.
[108] H. Lu, Z. Wu, I. Bhat, J. Electrochem. Soc. 144 (1997) L8.
[109] T. Takizawa, S. Arai, M. Nakahara, Jpn. J. Appl. Phys. 33 (1994) L643.
[110] Y. Wang, Y. Liu, H. Liang, Z. Mei, X. Du, Phys. Chem. Chem. Phys. 15 (2013) 2345.
[111] W. Wu, A. Katsnelson, O.G. Memis, H. Mohseni, Nanotechnology 18 (2007) 485302.
[112] W. Wu, D. Dey, O.G. Memis, A. Katsnelson, H. Mohseni, Nanoscale Res. Lett. 3 (2008) 123.
[113] W. Wu, D. Dey, O.G. Memis, A. Katsnelson, H. Mohseni, in: Proceedings of the Society of Photo-optical Instrumentation Engineers (SPIE), vol. 7614, 2010, p. 76140B.
[114] W. Wu, D. Dey, A. Katsnelson, O.G. Memis, H. Mohseni, J. Vac. Sci. Technol. B 26 (2008) 1745.
[115] W. Wu, D. Dey, O.G. Memis, A. Katsnelson, H. Mohseni, Nanoscale Res. Lett. 3 (2008) 351.
[116] K. Lee, W. Wagermaier, A. Masic, K.P. Kommareddy, M. Bennet, I. Manjubala, S.-W. Lee, S.B. Park, H. Cölfen, P. Fratzl, Nat. Commun. 3 (2012) 725.
[117] Z. Gemici, P.I. Schwachulla, E.H. Williamson, M.F. Rubner, R.E. Cohen, Nano Lett. 9 (2009) 1064.
[118] L. Zhang, Y. Li, J. Sun, J. Shen, Langmuir 24 (2008) 10851.
[119] D. Lee, Z. Gemici, M.F. Rubner, R.E. Cohen, Langmuir 23 (2007) 8833.
[120] K. Askar, B.M. Phillips, X. Dou, J. Lopez, C. Smith, B. Jiang, P. Jiang, Opt. Lett. 37 (2012) 4380.
[121] K.T. Cook, K.E. Tettey, R.M. Bunch, D. Lee, A.J. Nolte, ACS Appl. Mater. Interfaces 4 (2012) 6426.
[122] M. Ibn-Elhaj, M. Schadt, Nature 410 (2001) 796.
[123] S. Venkatesh, P. Jiang, B. Jiang, Langmuir 23 (2007) 8231.
[124] P. Zhu, G. Liu, J. Zhang, N. Tansu, J. Disp. Technol. 9 (2013) 317.
[125] R. Farrell, A. Al-Heji, C. Neufeld, X. Chen, M. Iza, S. Cruz, S. Keller, S. Nakamura, S. DenBaars, U. Mishra, Appl. Phys. Lett. 103 (2013) 241104.
[126] P. Papet, O. Nichiporuk, A. Kaminski, Y. Rozier, J. Kraiem, J.-F. Lelievre, A. Chaumartin, A. Fave, M. Lemiti, Sol. Energy Mater. Sol. Cells 90 (2006) 2319.
[127] M.D. Camras, M.R. Krames, W.L. Snyder, F.M. Steranka, R.C. Taber, J.J. Uebbing, D.W. Pocius, T.A. Trottier, C.H. Lowery, G.O. Mueller, Light emitting diodes with improved light extraction efficiency, in: Google Patents, 2006.
[128] H. Gauck, T. Gfroerer, M. Renn, E. Cornell, K. Bertness, Appl. Phys. A 64 (1997) 143.
[129] K. Lin, K.R. Catchpole, P. Campbell, M.A. Green, Semicond. Sci. Technol. 19 (2004) 1268.
[130] R.P. Martin, J. Velten, A. Stintz, K.J. Malloy, R.I. Epstein, M. Sheik-Bahae, M.P. Hasselbeck, B. Imangholi, S. Boyd, T.M. Bauer, in: Proceedings of the Society of Photo-optical Instrumentation Engineers (SPIE), vol. 6461, 2007, p. 6410H.
[131] A. Stintz, R.I. Epstein, M. Sheik-Bahae, K.J. Malloy, M.P. Hasselbeck, S.T. Boyd, in: Proceedings of the Society of Photo-optical Instrumentation Engineers (SPIE), vol. 6907, 2008, p. 690709.
[132] S.S. Oh, C.-G. Choi, Y.-S. Kim, Microelectron. Eng. 87 (2010) 2328.
[133] C.F. Bohren, D.R. Huffman, Absorption and Scattering of Light by Small Particles, John Wiley & Sons, 2008.
[134] L. Cao, P. Fan, A.P. Vasudev, J.S. White, Z. Yu, W. Cai, J.A. Schuller, S. Fan, M. L. Brongersma, Nano Lett. 10 (2010) 439.
[135] P. Spinelli, M. Verschuuren, A. Polman, Nat. Commun. 3 (2012) 692.
[136] T. Temple, G. Mahanama, H. Reehal, D. Bagnall, Sol. Energy Mater. Sol. Cells 93 (2009) 1978.
[137] X. Chen, B. Jia, J.K. Saha, B. Cai, N. Stokes, Q. Qiao, Y. Wang, Z. Shi, M. Gu, Nano Lett. 12 (2012) 2187.
[138] R. Santbergen, T. Temple, R. Liang, A. Smets, R. van Swaaij, M. Zeman, J. Opt. 14 (2012) 024010.
[139] C.L. Tan, S.J. Jang, Y.T. Lee, Opt. Exp. 20 (2012) 17448.
[140] J. Kumar, X. Wei, S. Barrow, A.M. Funston, K.G. Thomas, P. Mulvaney, Phys. Chem. Chem. Phys. 15 (2013) 4258.
[141] K. Aslan, Z. Leonenko, J.R. Lakowicz, C.D. Geddes, J. Phys. Chem. B 109 (2005) 3157.
[142] Q.-H. Wei, K.-H. Su, S. Durant, X. Zhang, Nano Lett. 4 (2004) 1067.
[143] R.M. Penner, J. Phys. Chem. B 106 (2002) 3339.
[144] J.L. Trompette, H. Vergnes, J. Phys. Chem. B 110 (2006) 14779.
[145] G. Lu, G. Zangari, Electrochim. Acta 51 (2006) 2531.
[146] B. Desiatov, I. Goykhman, U. Levy, Nano Lett. 14 (2014) 648.
[147] I.H. Nia, S.J. Jang, O.G. Memis, R. Gelfand, H. Mohseni, in: Proceedings of the Society of Photo-optical Instrumentation Engineers (SPIE), vol. 8809, 2013, p. 880918.
[148] G. Baffou, M. Kreuzer, F. Kulzer, R. Quidant, Opt. Exp. 17 (2009) 3291.
[149] G. Baffou, C. Girard, R. Quidant, Phys. Rev. Lett. 104 (2010) 136805.
[150] P. Spinelli, M. Hebbink, R. De Waele, L. Black, F. Lenzmann, A. Polman, Nano Lett. 11 (2011) 1760.
[151] J.B. Khurgin, Phys. Rev. Lett. 98 (2007) 177401.
[152] I. Gontijo, M. Boroditsky, E. Yablonovitch, S. Keller, U. Mishra, S. DenBaars, Phys. Rev. B 60 (1999) 11564.
[153] J.B. Khurgin, G. Sun, Appl. Phys. Lett. 96 (2010) 181102.